Volume 35 http://acousticalsociety.org/

176th Meeting of Acoustical Society of America 2018
Acoustics Week in Canada
Victoria, Canada
5-9 November 2018
Underwater Acoustics: Paper 5aUW7

Characterizing the seabed by using noise interferometry and time warping

Tsuwei Tan and Oleg A. Godin
Physics Department, Naval Postgraduate School, Monterey, CA, 93943; ttan1@nps.edu; oagodin@nps.edu

Adrien Lefebvre and Wandrille Beaute
EAOM, BCRM de Brest, Ecole Navale, CC600, F-29240, BREST, Cedex 9, FRANCE, 29160; lefebvre5.eleve@ecole-navale.fr; beaute.eleve@ecole-navale.fr

Boris G. Katsnelson and Marina Yarina
Marine Geosciences Department, Leon Charney School of Marine Sciences, University of Haifa, Haifa, ISRAEL, 349883; bkatsnels@univ.haifa.ac.il; yarina_marina@icloud.com

This paper investigates the feasibility of an approach to passive acoustic characterization of the seafloor in the coastal ocean, which is based on the synthesis of noise interferometry and time warping. Both methods are widely used but have not been applied together to solve geoacoustic inverse problems. The proposed technique includes three major steps. First, an approximation to deterministic Green's function (GF) is obtained by calculating cross-correlation function of noise recorded by spatially separated hydrophones. In the second step, time warping transform is applied to the noise cross-correlation function (NCCF) to extract dispersion curves of acoustic normal modes. The measured dispersion curves are inverted in the third step to retrieve geoacoustic parameters of the seafloor. Feasibility of the technique is evaluated using ambient and shipping noise records obtained in the Shallow Water '06 experiment. The results of the NCCFs inversion for sediment layer thickness and sound speed are found to be consistent with earlier results obtained in the same area using controlled sound sources.

Published by the Acoustical Society of America

 https://doi.org/10.1121/2.0000955

I. Introduction

Passive acoustic remote sensing has the advantage of being low-cost and eco-friendly. Previously, noise cross-correlation function (NCCF) was proven to provide an approximation to deterministic Green's function (GF) from measuring ambient noise [1–3]. Time warping was successfully applied to analyze acoustic fields due to compact sources and extract dispersion curves of normal modes, which are sensitive to environmental parameters [4, 5]. Bonnel et al. were the first to apply such signal processing technique for geoacoustic inversions in underwater acoustics by using controlled sound sources [5]. Here we apply time warping to GF estimates, which are obtained passively from measured two-point cross-correlations of ambient and shipping noise. This paper combines noise interferometry with the time warping technique to quantitatively characterize the seabed in shallow water.

The proposed approach conceptually includes three steps. The first step is to calculate the NCCF from ambient noise recorded at two horizontally separated hydrophones. The NCCF serves as the signal to probe the environment and replaces the impulse response typically measured in the active acoustic remote sensing of the ocean. At the second step, time warping is applied to NCCF to extract its normal mode components and measure the mode travel times as a function of frequency. The mode travel times between two hydrophones contain environmental information, including information on seabed properties. The third step consists in solving the inverse problem of retrieving geoacoustic parameters from the passively measured modal dispersion curves. This paper uses the data obtained during the Shallow Water '06 (SW'06) experiment to demonstrate the feasibility of the proposed approach to passive acoustic remote sensing of the seafloor.

II. Experimental data and NCCF

The data were collected from a seven-day recording of acoustic pressure by 33 hydrophones in the SW'06 experiment [6]. The site of the experiment is off the New Jersey coast as shown in Fig. 1(a). The NCCF $C(\tau)$ is calculated for 32 pairs of hydrophones. Here τ is the time lag between the time series of pressure recorded on the first and second hydrophone. The first hydrophone is from the SHARK horizontal line array (HLA), and the second hydrophone used in each pair is a single hydrophone unit called SHRU, as shown in Fig. 1(a). SHARK HLA consisted of 32 hydrophones with 15 m spacing. We will refer to the X-th hydrophone on the line array as HLA hydrophone X.

Figure 1(b) shows estimates of NCCF between the last HLA hydrophone, which is HLA hydrophone 32, and SHRU that are obtained using different averaging time. Deterministic features of the NCCF emerge and become increasingly clear as the averaging time increases from 1.75 to 7 days. In the 10–90 Hz frequency band considered, the NCCF estimates become stable after stacking of about 5 days of records. To improve the quality and convergence of the NCCF estimate, spectrum pre-whitening has been applied [2]. Using pressure recorded in N non-overlapping time windows, NCCF is evaluated in the frequency domain as

$$C(\omega) = \frac{1}{N}\sum_{n=1}^{N} \frac{P_{HLA,n}(\omega)P_{Shru,n}^{*}(\omega)}{\left|P_{HLA,n}(\omega)P_{Shru,n}^{*}(\omega)\right|}, \quad (1)$$

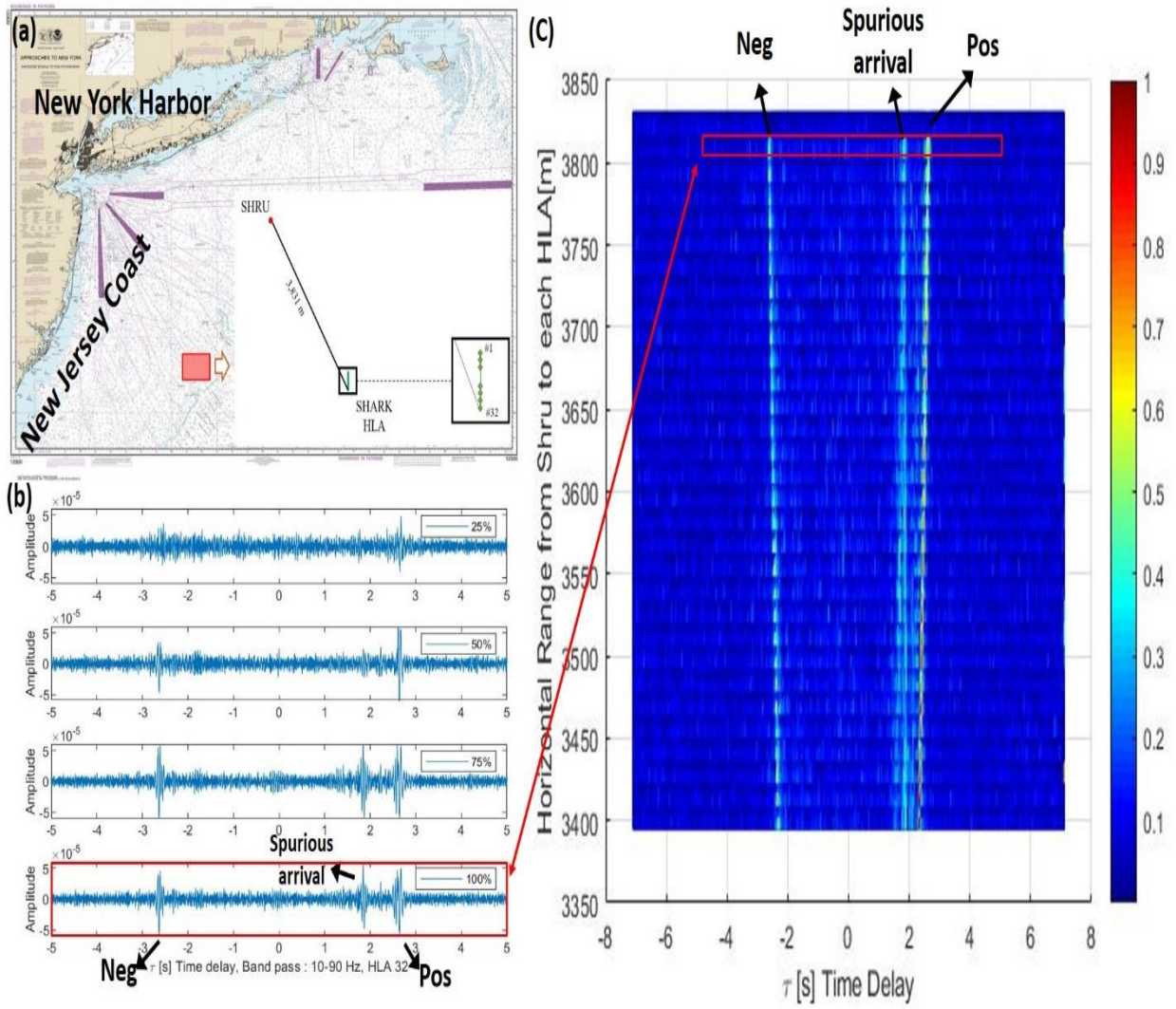

Fig. 1. Two-point cross-correlation functions of noise recorded during the SW'06 experiment. *(a) The general area and the site of the experiment. Purple lines show major shipping lanes, while the red rectangle indicates the experiment site. Relative positions of the single hydrophone receiving unit (SHRU) and horizontal line array (HLA) employed in this study are shown in two successive blow-ups in the right lower corner. (b) Emergence of a coherent signal structure from ambient noise. Estimates of cross-correlation of noise recorded by SHRU and HLA hydrophone 32 are shown for four different averaging times. The noise averaging time increases from 25% of the entire record to full 7 days' stacking. (c) Magnitude of normalized NCCF is shown by color as a function of time delay and the distance between HLA hydrophone and SHRU for all 32 HLA hydrophones. NCCFs are normalized so that the maximum of their absolute value equals 1 at each range shown. Note symmetric straight lines at positive and negative time delays, which are characteristic of cross-correlations of diffuse noise. An additional smaller peak at positive time delays is identified as a spurious arrival due to consistent low-frequency noise from New York harbor shipping. The red boxes in (b) and (c) represent the same NCCF.*

where $P_{HLA,n}(\omega)$ and $P_{Shru,n}(\omega)$ are spectra of the pressure recorded by respective hydrophones during the n-th time window. Time-domain NCCF $C(\tau)$ is obtained as a Fourier transform of Eq. (1). The spectrum pre-whitening helps suppress contributions of strong, transient non-diffuse noise sources such as nearby shipping.

Figure 1(c) shows the positions of the peaks that the measured NCCFs between SHRU and all HLA hydrophones have as a function of the time delay. As the horizontal separation between hydrophones in the NCCF pair changes, the absolute value of the time delay at the peaks increases linearly with range at both positive and negative τ, which is characteristic of the diffuse noise [1, 2, 7]. The peaks occur at the time delays, the absolute values of which correspond to acoustic travel times between the hydrophones. The close similarity of the positive- and negative-time-delay parts of NCCF extends to its fine structure as can be seen in Fig. 1(b). Red boxes in Figs. 1(b) and 1(c) indicate the same NCCF between SHRU and HLA hydrophone 32.

However, there is an additional peak appearing at the positive times before the main NCCF peak. We interpret the additional peak as a spurious arrival originating from a source of non-diffuse noise and attribute it to noise coming from the New York Harbor [8]. This is consistent with the time delay corresponding to the spurious arrival. In the following, we choose the negative time delay part of NCCF calculated from SHRU and HLA hydrophone 21 as input signal $C(\tau)$ for time warping as described in Section III.

III. Application of time warping transform to retrieve normal mode dispersion curves

Time warping is the process of transforming a signal $S(\tau)$ according to [4]

$$WS(\tau) = \sqrt{|w'(\tau)|}\, S\left[w(\tau)\right] . \tag{2}$$

Here $WS(\tau)$ is the warped signal, $w(\tau)$ is the warping function with the $\sqrt{|w'(\tau)|}$ term conserving the energy between the original and the warped signals. The warping function is

$$w(\tau) = \sqrt{\tau^2 + {\tau_r}^2} \ , \tag{3}$$

where $\tau_r = r / c_w$, with r being the range between two hydrophones and c_w being the water column sound speed. Equation (2) and (3) were derived for isospeed waveguide with perfectly reflecting boundaries.

In the context of noise interferometry, $S(\tau)$ is either the positive time-delay part, $S(\tau) = C(\tau),\ \tau > 0,$ or the negative time-delay part $S(\tau) = C(-\tau),\ \tau > 0,$ of the time-domain NCCF $C(\tau)$, which is obtained as the Fourier Transform of Eq. (1). Figure 2(a) shows the negative time delay part of NCCF, calculated for SHRU and HLA hydrophone 21. In Eq. (3), τ_r has the meaning of the emission time of the signal being warped. For the waveguide with depth-dependent sound speed, we need to perturb τ_r to find the optimal value of c_w in this non-ideal waveguide. Equation (2) transforms $C(\tau)$ to $WC(\tau)$ in the warped domain as shown in Figs. 2(a)–2(c). Figures 2(b) and 2(d) are the time-frequency representation of Figs. 2(a) and 2(c),

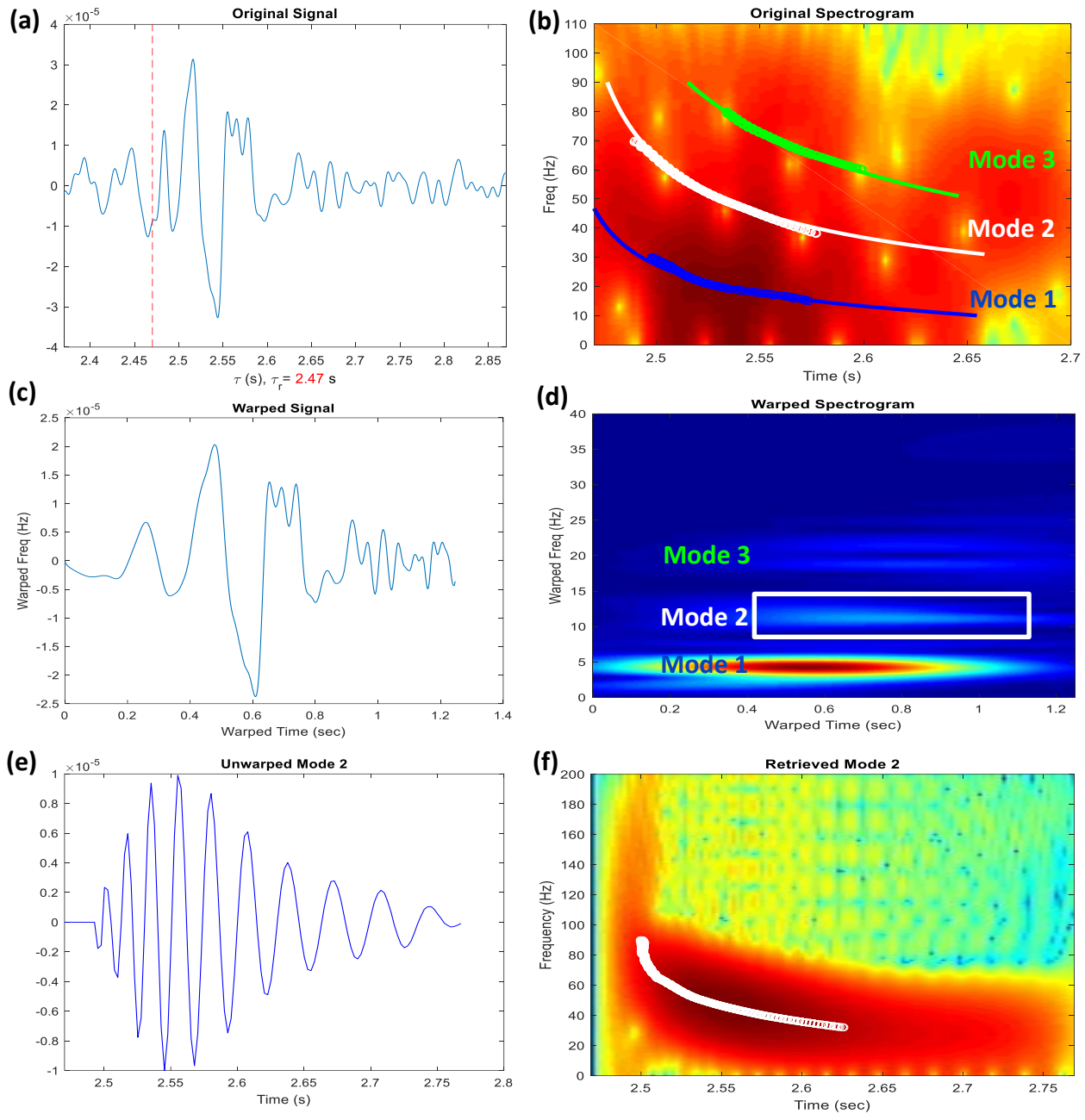

Fig. 2. Application of time warping to noise cross-correlations for retrieval of normal mode dispersion curves. *(a) Negative time-delay part of NCCF, which approximates Green's function and serves as the waveform of the received signal. (b) Spectrogram of NCCF with superimposed best-match modal dispersion curves that are obtained in the course of a geoacoustic inversion. Note that normal modes are not separated in the spectrogram in the physical domain. (c) NCCF after application of the warping transform. (d) Spectrogram of the warped signal. Note that normal modes are separated in the warped domain. The white box shows a time-frequency mask to isolate mode 2 for subsequent unwarping. (e) Mode 2 component of the NCCF retrieved using time warping. (f) Spectrogram of mode 2 component of NCCF. The white circles show the mode dispersion curve retrieved from the spectrogram.*

respectively. The best τ_r in Fig. 2(a) can be identified and further adjusted once the warped modes are fully resolved into three modes in the warped spectrogram as shown in Fig. 2(d).

Time warping is an invertible process between the physical domain and warped domain. After isolating the selected mode in the warped domain, it can be unwarped back to the original physical domain. The unwarping process $w^{-1}(\tau)=\sqrt{\tau^2-\tau_r{}^2}$ is applied from Fig. 2(d) to restore each individual mode as shown in Fig. 2(e). Here mode 2 is used as an example of a modal filtering scheme and unwarping, and its restored spectrogram is shown in Fig. 2(f) with measured dispersion curve shown by white circles. The dispersion curve of each mode was retrieved from its reassigned spectrogram [9] by finding the travel time that maximizes the spectrum in each frequency bin. Dispersion curves serve as input information for the geoacoustic inversion discussed in Section IV.

IV. Geoacoustic inversion

We model our environment as a sediment layer over a homogeneous half-space, as shown in Fig. 3(a). The effects of shear rigidity and absorption are neglected in modeling travel time of acoustic normal modes. The sound speed profile in the water column corresponds to the average of 7 days of *in situ* measurements during acoustic observations [6]. The inversion minimizes the following cost function:

$$\sum_{m,n=1}^{M,N}\left[\hat{t}_m\left(f_n,U\right)-t_m\left(f_n,U\right)\right]^2 \tag{4}$$

where $M=3$ is the number of normal modes to be identified, and N is the number of frequency components to be compared between theoretical and measured dispersion curves. U is a vector of 6 parameters, including range r between two hydrophones, and 5 geoacoustic parameters: sediment sound speed C_s, sediment density ρ_s, sediment thickness H, basement sound speed C_b, and basement density ρ_b. The range r between SHRU and HLA hydrophone 21 is known to be about 3675m but not to the accuracy required in the geoacoustic inversion, so r is adjusted in the course of the inversion. $\hat{t}_m\left(f_n,\hat{U}\right)$ is the extracted experimental travel time of each mode m at a particular frequency component n. The theoretical modal travel time of each frequency component $t_m\left(f_n,U\right)$ is calculated by the normal mode code KRAKEN [10].

We have used an exhaustive search to minimize the cost function Eq. (4) and find the vector U_{min}, which represents the inferred value of the six-dimensional vector $\hat{U}$. Table 1 gives the parameter search bounds and summarizes the result. To better understand the result, Fig. 3(b) illustrates the analysis of the cost function sensitivity to sediment sound speed C_s, as an example of inversion for the 6 unknown parameters. Each black dot shows root-mean-square (RMS) difference between measured and predicted modal travel times for a particular set U of model parameters. C_s value in each set is shown in Fig. 3(b). The red circle in Fig. 3(b) indicates the black dot which minimizes the cost function and determines the inferred value of $\hat{U}$. Figure 3(b)

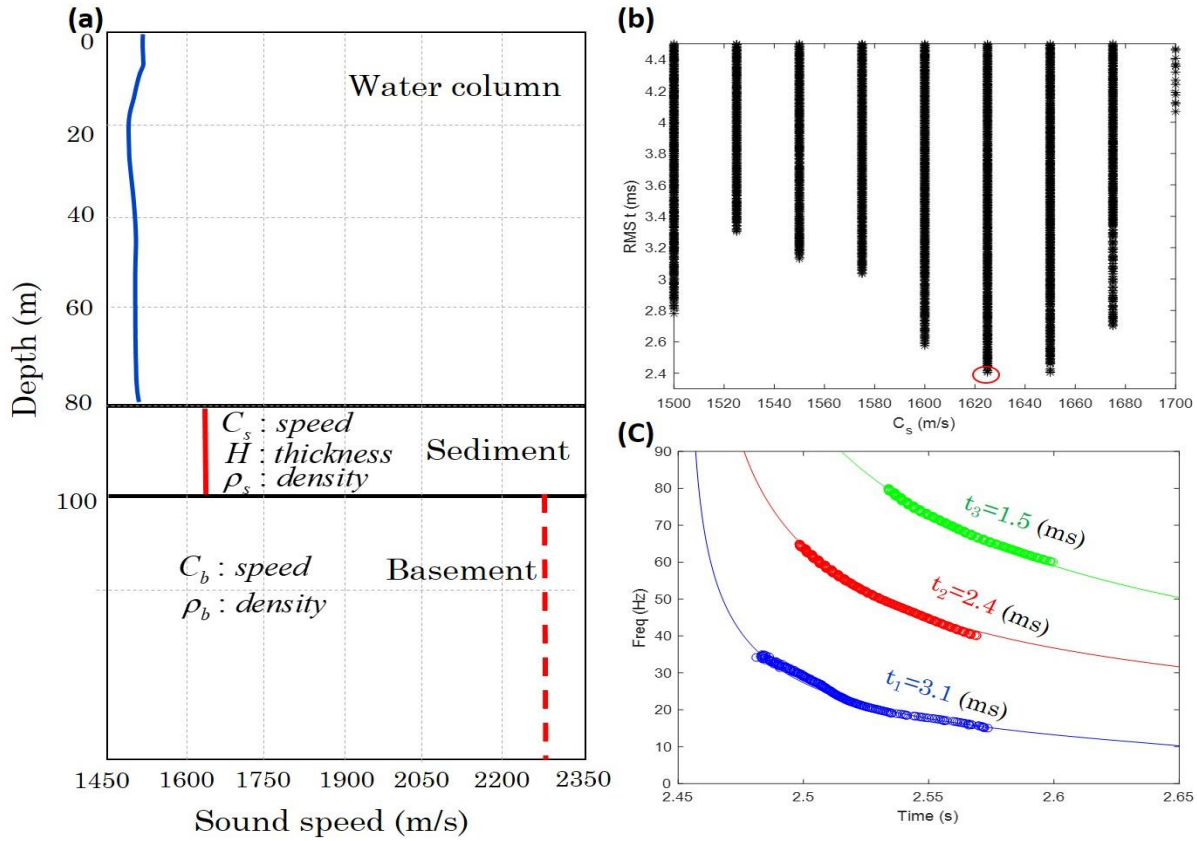

Fig. 3. Geoacoustic inversion. *(a) Environmental model implied in the inversion process. Sound speed profile in water (blue line) and water depth are assumed to be known. Distance between hydrophones and 5 geoacoustic parameters (sound speeds and densities in the sediment layer and the basement as well as sediment layer thickness) were the unknown parameters to be determined. (b) Sensitivity of root-mean-square mode travel time discrepancy to sediment sound speed. The dots represent the mismatch as function of C_s for various values of the other unknown parameters, and the red circle is the minimum mismatch at the inverted value of C_s. (c) Comparison of modeled (lines) and measured (circles) dispersion curves for the optimal set of inverted parameters. Root-mean-square errors in milliseconds between modeled and measured travel times are shown for each of the first three normal modes.*

Table 1. Summary of inversion results.

Parameter	Unit	Search bounds	Step	Inverted Result
r	m	[3650, 3685]	1	3658
C_s	m/s	[1500, 1700]	25	1625
ρ_s		[1.1, 1.9]	0.2	1.3
H	m	[5, 30]	5	20
C_b	m/s	[1700, 2400]	25	2275
ρ_b		[1.3, 2.5]	0.2	1.5

shows the value of C_s in the best-matching environmental model and also illustrates the rate of increase in the travel time discrepancy with C_s deviation from its optimum value.

Range between two hydrophones r is underestimated by 16m relative to the nominal range value, or up to one wavelength in our frequency band. Range discrepancy is less than 0.5% of the nominal range, and it meets the uncertainty of measurements of hydrophone positions from GPS coordinates in the experiment.

Previously, a number of geoacoustic inversion studies were performed at the SW'06 experiment site using controlled compact sources [5, 11–15]. These studies have been reviewed by Chapman [16] and Frisk et al. [17]. The normal mode dispersion curves retrieved using time warping are most sensitive to the parameters C_s and H_s of the sediment layer. The inferences of the sound speed in a homogeneous sediment layer and the layer's thickness range between 1600–1650 m/s and 20–25 m, respectively, in the previous studies [16]. Our inverted sediment sound speed C_s and sediment thickness H from Table 1 fall within these bounds. However, our estimate of the basement sound speed C_b is significantly higher than the 1700 m/s value reported in Ref. [14]. This can be attributed, in part, to weak penetration of acoustic energy into the bottom below the 20-meter sediment layer, which leads to a weak sensitivity of the normal mode travel times, at frequencies away from the mode cutoff frequencies, to the basement sound speed C_b and density ρ_b. Another likely reason for the difference in C_b inferences is the difference in the acoustic frequencies employed by Jiang et al. [14] and in this study. Midfrequency (1500–4500 Hz) chirps were used in Ref. [14], while noise interferometry provides virtual sound sources with frequencies below 100 Hz with peak energy densities below 30 Hz, as seen in Fig. 2(b). The low-frequency virtual sound source is able to interrogate deeper sub-bottom layers.

Moreover, the marine geology data reviewed in Ref. [17] indicate that the simple sediment-layer-over-half-space geoacoustic model is an oversimplification of the ocean bottom structure at the SW'06 experiment site. Our geoacoustic model does not allow for the second, "slow" sediment layer [17] between the upper sediment layer and fast sub-bottom. Very high C_b values in our model are needed to match the observed deep minima of the mode group speeds, which occur slightly above respective cutoff frequencies. Arguably, the unrealistically high C_b values in the model mimic the effect of the unresolved slow sediment layer on the group speeds.

Overall, results of our ambient-noise-based, passive geoacoustic inversion are consistent with the results for sediment layer thickness and sound speed obtained using controlled sound sources.

V. Conclusion

We have demonstrated the feasibility of a novel approach to acoustic characterization of the ocean bottom in a shallow-water waveguide. The approach is passive and uses two-point cross-correlation function of ambient and distant shipping noise as the source of information about the environment. This information is retrieved from the acoustic pressure fluctuations by using a time-warping transform to isolate normal mode components of the noise cross-correlation function. Using the data obtained in the SW'06 experiment, we showed that at ranges of 40–50 water depths, measured NCCFs provide an approximation of the deterministic Green's function, which is sufficiently accurate to describe inter- and intra-mode dispersion. Dispersion curves of three lowest-order normal modes were successfully retrieved from two-point cross-correlation

function of noise and inverted for geoacoustic parameters of the seafloor at the SW'06 experiment site. The results of the passive geoacoustic inversion for sediment layer parameters are largely consistent with the earlier results, which were obtained using various controlled compact sources to probe the seafloor.

Acknowledgements

The data used in this study were collected by the Woods Hole Oceanographic Institution and provided to us by Arthur Newhall. The authors gratefully acknowledge Dr. Julien Bonnel's advice on implementation of the time warping transform. Constructive criticism by Dr. Megan Ballard helped us to improve presentation. This work was supported in part by the National Science Foundation, grant No. OCE1657430, and the Office of Naval Research, award No. N00014-18-WX-01725.

References

[1] P. Roux, W. A. Kuperman, and NPAL Group, "Extracting coherent wave fronts from acoustic ambient noise in the ocean," J. Acoust. Soc. Am. **116**, 1995–2003 (2004).

[2] X. Zang, M. G. Brown, and O. A. Godin, "Waveform modeling and inversion of ambient noise cross-correlation functions in a coastal ocean environment." J. Acoust. Soc. Am. **138**, 1325–1333 (2015)

[3] O. A. Godin, B. G. Katsnelson, J. Qin, M. G. Brown, N. A. Zabotin, and X. Zang, "Application of Time Reversal to Passive Acoustic Remote Sensing of the Ocean." Acoust. Phys. **63**, 309–320 (2017)

[4] J. Bonnel, B. Nicolas, J.I. Mars and S.C. Walker, "Geoacoustic inversion in a dispersive waveguide using warping operators," J. Acoust. Soc. Am. **128**, 719–727 (2010).

[5] J. Bonnel, and N. R. Chapman, "Geoacoustic inversion in a dispersive waveguide using warping operators." J. Acoust. Soc. Am. **130**, EL101–EL107 (2011).

[6] A. E. Newhall, T. F. Duda, K. vond der Heydt, J. D. Irish, J. N. Kemp, S. A. Lerner, S. P. Liberatore, Y.T. Lin, J. F. Lynch, A. R. Maffei, A. K. Morozov, Al Shmelev, C. J. Sellers, and W. E. Witzell, "Acoustic and Oceanographic Observations and Configuration Information for the WHOI Moorings from the SW06 Experiment." No. WHOI-2007-04. Woods Hole Oceanographic Institution MA (2007).

[7] M.G. Brown, O.A. Godin, X. Zang, J.S. Ball, N.A. Zabotin, L.Y. Zabotina, and N.J. Williams, "Ocean acoustic remote sensing using ambient noise: results from the Florida Straits." Geophys. J. Int. **206**, 574–589 (2016).

[8] J. X. Qin, B. G. Katsnelon, O. A. Godin and Z. L. Li," Geoacoustic Inversion Using Time Reversal of Ocean Noise" Chin. Phys. Lett. **34** (9) 094301 (2017).

[9] F. Auger and P. Flandrin, "Improving the readability of time-frequency and time-scale representations by the reassignment method," Trans. Signal Process. **43**, 1068–1089 (1995).

[10] M. Porter, The KRAKEN Normal Mode Program, http://oalib.hlsresearch.com/Modes/AcousticsToolbox/manual_html/kraken.html

[11] Y. Jiang, and N. R. Chapman, "Bayesian geoacoustic inversion in a dynamic shallow water environment," J. Acoust. Soc. Am **123**, EL155–EL161 (2008).

[12] J.W. Choi, P.H. Dahl, and J.A. Goff, "Observations of the R reflector and sediment interface reflection at the Shallow Water'06 Central Site," J. Acoust. Soc. Am. **124**, EL128–EL134 (2008).

[13] M.S. Ballard, K.M. Becker, and J.A. Goff, "Geoacoustic inversion for the New Jersey shelf: 3-D sediment model," IEEE J. Oceanic Eng. **35**, 28–42 (2010).

[14] Y. Jiang, N. R. Chapman, and P. Gerstoft, "Estimation of geoacoustic properties of marine sediment using a hybrid differential evolution inversion method," IEEE J. Oceanic Eng. **35**, 59–69 (2010).

[15] C.F. Huang, P. Gerstoft, and W.S. Hodgkiss, "Effect of ocean sound speed uncertainty on matched-field geoacoustic inversion," J. Acoust. Soc. Am. **123**, EL162–EL168 (2010).

[16] N.R. Chapman, "An experimental benchmark for geoacoustic inversion methods," J. Acoust. Soc. Am. **142**, 2621 (2017).

[17] G.V. Frisk, K.M. Becker, S.D. Rajan, C.J. Sellers, K.Von Der Heydt, C.M. Smith, and M.S. Ballard, "Modal mapping experiment and geoacoustic inversion using sonobuoys," IEEE J. Oceanic Eng. **40** (3), 607–620 (2015)